CHALMERS
UNIVERSITY OF TECHNOLOGY

A parsec-scale radio jet launched by the central intermediate-mass black hole in the dwarf galaxy SDSS J090613.77+561015.2

Monthly Notices
of the
ROYAL ASTRONOMICAL SOCIETY

MNRAS **495,** L71–L75 (2020)
Advance Access publication 2020 April 7

doi:10.1093/mnrasl/slaa052

A parsec-scale radio jet launched by the central intermediate-mass black hole in the dwarf galaxy SDSS J090613.77+561015.2

Jun Yang [1★] Leonid I. Gurvits,[2,3,4] Zsolt Paragi,[2] Sándor Frey [5,6] John E. Conway,[1] Xiang Liu[7] and Lang Cui[7]

[1]*Department of Space, Earth and Environment, Chalmers University of Technology, Onsala Space Observatory, SE-43992 Onsala, Sweden*
[2]*Joint Institute for VLBI ERIC, Oude Hoogevceensedijk 4, NL-7991 PD Dwingeloo, the Netherlands*
[3]*Department of Astrodynamics and Space Missions, Delft University of Technology, Kluyverweg 1, NL-2629 HS Delft, the Netherlands*
[4]*CSIRO Astronomy and Space Science, PO Box 76, Epping, NSW 1710, Australia*
[5]*Konkoly Observatory, Research Centre for Astronomy and Earth Sciences, Konkoly Thege Miklós út 15-17, H-1121 Budapest, Hungary*
[6]*Institute of Physics, ELTE Eötvös Loránd University, Pázmány Péter sétány 1/A, H-1117 Budapest, Hungary*
[7]*Xinjiang Astronomical Observatory, Key Laboratory of Radio Astronomy, Chinese Academy of Sciences, 150 Science 1-Street, 830011 Urumqi, P.R. China*

Accepted 2020 March 23. Received 2020 March 23; in original form 2020 March 12

ABSTRACT

The population of intermediate-mass black holes (IMBHs) in nearby dwarf galaxies plays an important 'ground truth' role in exploring black hole formation and growth in the early Universe. In the dwarf elliptical galaxy SDSS J090613.77+561015.2 ($z = 0.0465$), an accreting IMBH has been revealed by optical and X-ray observations. Aiming to search for possible radio core and jet associated with the IMBH, we carried out very long baseline interferometry (VLBI) observations with the European VLBI Network at 1.66 GHz. Our imaging results show that there are two 1-mJy components with a separation of about 52 mas (projected distance 47 pc) and the more compact component is located within the 1σ error circle of the optical centroid from available *Gaia* astrometry. Based on their positions, elongated structures and relatively high brightness temperatures, as well as the absence of star-forming activity in the host galaxy, we argue that the radio morphology originates from the jet activity powered by the central IMBH. The existence of the large-scale jet implies that violent jet activity might occur in the early epochs of black hole growth and thus help to regulate the co-evolution of black holes and galaxies.

Key words: galaxies: active – galaxies: dwarf – galaxies: individual: SDSS J090613.77+561015.2 – galaxies: jets – radio continuum: galaxies.

1 INTRODUCTION

The population of low-mass black holes (BHs) in nearby dwarf galaxies, i.e. galaxies with $M_{\rm g} \leq 10^{9.5}\,{\rm M}_{\odot}$, plays a key role in shedding light on BH formation and growth in the early Universe. One of the reasons of such a role is related to the fact that the probability of undergoing merging events in the population of dwarf galaxies is lower than for their larger counterparts, and therefore the masses of their central BHs are likely to remain close to their 'birth' values (e.g. Reines & Comastri 2016; Greene, Strader & Ho 2020). These BHs with masses of $10^2\,{\rm M}_{\odot} \leq M_{\rm bh} \leq 10^6\,{\rm M}_{\odot}$ are typically classified as intermediate-mass black holes (IMBHs). Finding and weighing them would enable us to distinguish between different BH seed formation mechanisms, those involving a direct collapse at the mass level of $M_{\rm bh} \sim 10^4\,{\rm M}_{\odot}$ and population III star seeds with a typical mass of $M_{\rm bh} \sim 10^2\,{\rm M}_{\odot}$ (e.g. the simulation by Volonteri 2010).

At present, there are several hundred accreting IMBH candidates in dwarf galaxies that exhibit optical spectroscopic or X-ray signatures (fraction <1 per cent, Reines, Greene & Geha 2013; Pardo et al. 2016). Among them, only a small number of IMBHs (e.g. 12 in Schutte, Reines & Greene 2019) have been identified in dwarf galaxies hosting active galactic nuclei (AGNs).

About 0.3 per cent of dwarf galaxies have radio counterparts (Reines et al. 2020) in the FIRST (Faint Images of the Radio Sky at Twenty Centimeters, Becker, White & Helfand 1995) survey. High-resolution very long baseline interferometry (VLBI) observations of these radio counterparts provide direct insight in their nature and mechanism of emission, involving non-thermal radio jet/outflow activity. Both jets and wide opening angle winds

★ E-mail: jun.yang@chalmers.se

are major ingredients in the feedback mechanisms that are reflected in the co-evolution between BHs and galaxy bulges, i.e. the $M_{\rm bh}$–σ correlation in which σ is the stellar velocity dispersion (e.g. Kormendy & Ho 2013; Greene et al. 2020) and the $M_{\rm bh}$–$M_{\rm bulge}$ correlation (e.g. Schutte et al. 2019). Revealing radio AGN activity would enable us to probe the feedback of the IMBHs (e.g. Manzano-King, Canalizo & Sales 2019; Greene et al. 2020). In addition, VLBI detections of compact radio cores would provide data points for filling the gap between supermassive and stellar mass BHs for testing the mass-dependent relations (e.g. the Fundamental Plane relation, Yuan & Narayan 2014) and allow us to search for off-nuclear IMBHs (Reines et al. 2020) formed by galaxy mergers (e.g. Bellovary et al. 2019). To date, there are some high-resolution imaging observations of IMBHs, e.g. POX 52 (Thornton et al. 2008), Henize 2–10 (Reines & Deller 2012), and NGC 404 (Paragi et al. 2014). However, radio jets or steady radio-emitting polar outflows, compact on sub-pc scales, have been revealed in only one dwarf galaxy, NGC 4395 (Wrobel & Ho 2006).

The dwarf elliptical galaxy SDSS J090613.77+561015.2 at the redshift $z = 0.0465$ hosts an AGN and has a stellar mass of $2.3 \times 10^9\,{\rm M}_\odot$ (source ID: 9, Reines et al. 2013). It displays not only some narrow-line AGN signatures but also a persistent broad Hα emission (source ID: RGG 9, Baldassare et al. 2016). Based on high spectral resolution observations, Baldassare et al. (2016) estimated the mass of its BH as $M_{\rm bh} = 3.6^{+5.9}_{-2.3} \times 10^5\,{\rm M}_\odot$ (including the systematic uncertainty of 0.42 dex). In the long-slit spectroscopy with the Keck I telescope, it shows some spatially extended ionized gas outflows that are most likely AGN-driven because their velocity (701 ± 7 km s^{-1}) exceeds the escape velocity (303 ± 35 km s^{-1}) of its halo (Manzano-King et al. 2019). It is a slightly resolved point-like source with total the flux density of 22.4 ± 4.1 mJy in the GMRT (Giant Metrewave Radio Telescope) 150 MHz all-sky radio survey (Intema et al. 2017) and 4.7 ± 0.2 mJy in the 1.4 GHz FIRST survey (Becker et al. 1995). It has a flux density of 0.93 ± 0.05 mJy at 9.0 GHz and 0.78 ± 0.04 mJy at 10.65 GHz in the Karl G. Jansky Very Large Array (VLA) observations (source ID: 26, Reines et al. 2020).

This Letter is composed as follows. In Section 2, we describe our European VLBI Network (EVN) observations and data reduction. In Section 3, we present the high-resolution imaging results. In Section 4, we discuss the physical nature of the detected components and the implication from our findings. Throughout the paper, a standard Λ cold dark matter cosmological model with $H_0 = 71$ km s^{-1} Mpc^{-1}, $\Omega_{\rm m} = 0.27$, $\Omega_\Lambda = 0.73$ is adopted; the VLBI images then have a scale of 0.9 pc mas^{-1}.

2 VLBI OBSERVATIONS AND DATA REDUCTION

We observed SDSS J090613.77+561015.2 for 2 h on 2017 January 17 with the e-EVN and for 12 h on 2017 November 6 with the full EVN. Both observations used the standard 1-Gbps experiment set-up (16 sub-bands, 16 MHz bandwidth per sub-band, dual circular polarization, 2-bit quantization) at the frequency of 1.66 GHz. The participating telescopes were Jodrell Bank Mk2 (Jb), Westerbork (Wb, single dish), Effelsberg (Ef), Medicina (Mc), Onsala (O8), Tianma (T6), Urumqi (Ur), Toruń (Tr), Svetloe (Sv), Zelenchukskaya (Zc), and Badary (Bd). Table 1 gives the observing time and the used stations at each epoch. The correlation was done by the EVN software correlator (SFXC, Keimpema et al. 2015) at JIVE (Joint Institute for VLBI, ERIC) using standard correlation parameters of continuum experiments.

Table 1. Summary of the 1.66 GHz EVN observations of SDSS J090613.77+561015.2.

Observing date and time	Project code and participating stations
2017 Jan 17, 18–20 h UT	RSY05: JbWbEfMcO8TrT6
2017 Nov 6, 00–12 h UT	EY029: JbWbEfMcO8TrT6UrSvZcBd

Both experiments were performed in the phase-referencing mode to gain the calibration solutions and a reference position for our faint target. The bright source J0854+5757, about 2.°4 apart from SDSS J090613.77+561015.2 and a key source in the International Celestial Reference Frame (Ma et al. 1998), was observed periodically as the phase-referencing calibrator. The calibrator has a J2000 position at RA $= 08^{\rm h}54^{\rm m}41.^{\rm s}996408$ ($\sigma_{\rm ra} = 0.2$ mas), Dec. $= 57^\circ57'29.''93914$ ($\sigma_{\rm dec} = 0.1$ mas) in the source catalogue of 2015a from the Goddard Space Flight Centre VLBI group.[1] The calibrator position has an offset of 0.7 mas with respect to the optical position in the second data release (DR2, Gaia Collaboration 2018) of the *Gaia* mission (Gaia Collaboration 2016). The nodding observations used a duty-cycle period of about 5 min (1 min for J0854+5757, 3 min for SDSS J090613.77+561015.2, 1 min for two scan gaps). During the observations, the sources was at an elevation of $\geq 18^\circ$ at all European telescopes.

The visibility data were calibrated using the National Radio Astronomy Observatory (NRAO) Astronomical Image Processing System (AIPS version 31DEC17, Greisen 2003) software package. We removed the visibility data of side channels because of their low correlation amplitude while loading the data into AIPS and then ran the task ACCOR to re-normalize the correlation amplitude. A priori amplitude calibration was performed with the system temperatures and the antenna gain curves if provided by the telescopes. If these data were missing, the nominal values were used. The ionospheric dispersive delays were corrected according to the map of total electron content provided by the Global Positioning System satellite observations. Phase errors due to the antenna parallactic angle variations were removed. After a manual phase calibration was carried out, the global fringe-fitting and bandpass calibration were performed.

The calibrator J0854+5757 was imaged using iterations of model fitting with a group of point sources (delta functions) and self-calibration (Stokes *I*) in the software package DIFMAP (version 2.5e, Shepherd, Pearson & Taylor 1994), fringe-fitting and self-calibration (Stokes *RR* and *LL*) in AIPS. The calibrator had a single-sided core–jet structure with a total flux density of 0.61 ± 0.03 Jy in the first observing epoch. Due to a firmware bug in the European digital base-band converters, there were significant sensitivity losses in the second epoch. According to the long-term light curve at 15 GHz observed by the 40-m telescope at the Owens Valley Radio Observatory (Richards et al. 2011) and published online,[2] the calibrator had stable flux densities in 2017. Assuming that the calibrator had no flux density variation between the two epochs, we derived an amplitude correction factor of 1.63 in the imaging procedures. We used the jet base, the brightest component, as the reference point in the phase-referencing calibration. After about 10 iterations, the deconvolved map of Stokes *I* using natural weighting reached an image noise level of 0.016 mJy beam^{-1}, as low as the map of zero-flux-density Stokes *V*. The core–jet structure in the

[1] http://astrogeo.org/vlbi/solutions/rfc_2015a/
[2] http://www.astro.caltech.edu/ovroblazars

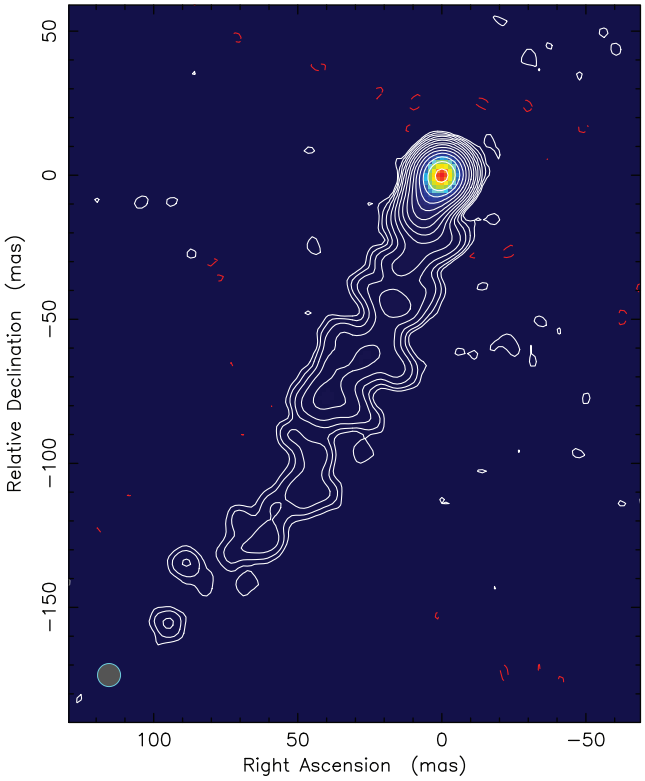

Figure 1. The jet structure of the phase-referencing calibrator J0854+5757. The 1.66-GHz EVN image has a dynamic range of $\frac{S_{\rm pk}}{\sigma_{\rm rms}} = 30\,250$. The contours start at 0.016 mJy beam^{-1} (3σ) and increase by a factor of 2. The peak brightness is 484 mJy beam^{-1}. To properly show the faint jet structure, we used a large circular restoring beam with an FWHM of 8 mas.

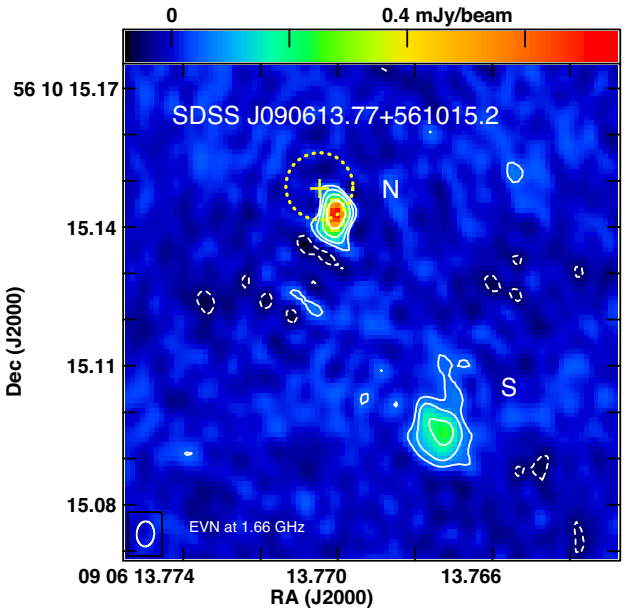

Figure 2. A two-component brightness distribution found by the EVN at 1.66 GHz in the dwarf galaxy SDSS J090613.77+561015.2 hosting an accreting IMBH. The yellow cross and circle mark the optical (*Gaia* DR2) centroid and the total 1σ error, respectively. The contours start at 0.048 mJy beam^{-1} (3σ) and increase by a factor of 2. The peak brightness is 0.76 mJy beam^{-1}. The restoring beam is 5.81 mas × 4.05 mas (FWHM) at $-3.^{\circ}03$ position angle and plotted in the bottom-left corner.

phase-referencing calibrator J0854+5757 observed in the second epoch is shown in Fig. 1. In the final high dynamic range image, 82 positive point sources were used. Both the phase and amplitude self-calibration solutions were also transferred and applied to the target source. In the residual map of the target source, there are no clearly seen systematic errors (noise peaks, strips, and rings). This indicates that the phase-referencing calibration worked properly.

3 RADIO STRUCTURE IN SDSS J090613.77+561015.2

The full-EVN image of SDSS J090613.77+561015.2 obtained on 2017 November 6 is shown in Fig. 2. There are two components detected and labelled as N and S in the CLEAN map. The optical centroid, reported by the *Gaia* DR2 (Gaia Collaboration 2018), is marked as a yellow cross (J2000, RA = $09^{\rm h}06^{\rm m}13\overset{\rm s}{.}77047$, Dec. = $56^{\circ}10'15\overset{''}{.}1482$, $\sigma_{\rm ra} = \sigma_{\rm dec.} = 0.8$ mas, the astrometric excess noise to set the reduced $\chi^2_{\rm r} = 1$ is 7.0 mas). The large excess noise is most likely related to the extended optical morphology and a certain level of asymmetric brightness distribution in the bulge (Schutte et al. 2019). The total error, added in quadrature, is shown as a dotted yellow circle. The two components are also detected in the first short e-EVN observations. Due to its relatively low image quality, that image is not shown here.

In order to determine the parameters of the obtained brightness distribution, we fitted two circular Gaussian components to the visibility data using DIFMAP. The model-fitting results including the 1σ formal uncertainties at the reduced $\chi^2_{\rm r} = 1$ are listed in Table 2.

The systematic error of $S_{\rm pk}$, $S_{\rm obs}$, and $L_{\rm R}$ are about 10 per cent. Using J0854+5757 as reference, we estimate the coordinates of the component N as RA = $09^{\rm h}06^{\rm m}13\overset{\rm s}{.}77005$ and Dec. = $56^{\circ}10'15\overset{''}{.}1429$ with a total systematic error <1 mas. The component N is partly resolved and has a faint (∼0.2 mJy) extension of about 4 mas towards south. The separation between the components N and S is 52.3 ± 0.3 mas. With respect to the component N, the component S has a position angle of about -154°.

All the available to date total flux density measurements of the source SDSS J090613.77+561015.2 are plotted in Fig. 3. Assuming no flux density variability, we fit the blue data points collected from the literature (Becker et al. 1995; Intema et al. 2017; Reines et al. 2020) to a power-law spectrum $S_\nu = S_0\nu^\alpha$ and determine $S_0 = 5.94 \pm 0.39$ mJy, the spectral index $\alpha = -0.84 \pm 0.04$. According to this model, SDSS J090613.77+561015.2 has a total flux density of 3.9 ± 0.3 mJy at 1.66 GHz. Compared to this estimate, the high-resolution EVN image recovers only about 50 per cent. We also tried to search for diffuse radio emission. On the shortest baseline Ef–Wb, there is a hint for a faint and diffuse structure connecting the two components and extending farther on both sides. However, because of the lack of the shorter baselines, it is hard to make a reliable image for the diffuse structure from the available data. The existence of the diffuse radio structure is also expected since the source is slightly resolved (deconvolved FWHM: $2\overset{''}{.}1 \times 1\overset{''}{.}1$ in the major axis position angle 40°) in the VLA FIRST image (Becker et al. 1995) and the elongation direction is roughly consistent with the overall EVN morphology extent.

The next to last column in Table 2 presents an average brightness temperature, estimated as (e.g. Condon et al. 1982)

$$T_{\rm b} = 1.22 \times 10^9 \frac{S_{\rm obs}}{\nu^2_{\rm obs}\theta^2_{\rm size}}(1+z), \quad (1)$$

Table 2. Summary of the circular Gaussian model-fitting results. Columns give (1) epoch, (2) component name, (3) peak brightness, (4) integrated flux density, (5–6) relative offsets in right ascension and declination with respect to component N, (7) deconvolved angular size (FWHM), (8) brightness temperature, and (9) radio luminosity.

Epoch	Name	$S_{\rm pk}$ (mJy beam^{-1})	$S_{\rm obs}$ (mJy)	$\Delta\alpha\cos\delta$ (mas)	$\Delta\delta$ (mas)	$\theta_{\rm size}$ (mas)	$T_{\rm b}$ (K)	$L_{\rm R}$ erg s^{-1}
1	N	0.616 ± 0.022	0.94 ± 0.06	0.00 ± 0.20	0.00 ± 0.28	2.14 ± 0.12	9.5×10^7	7.7×10^{37}
1	S	0.428 ± 0.022	1.04 ± 0.06	-21.06 ± 0.44	-51.14 ± 0.57	4.10 ± 0.32	2.9×10^7	8.5×10^{37}
2	N	0.781 ± 0.016	0.88 ± 0.02	0.00 ± 0.04	0.00 ± 0.05	1.82 ± 0.14	1.2×10^8	7.2×10^{37}
2	S	0.449 ± 0.016	0.98 ± 0.04	-22.47 ± 0.21	-47.19 ± 0.21	8.02 ± 0.42	7.1×10^6	8.0×10^{37}

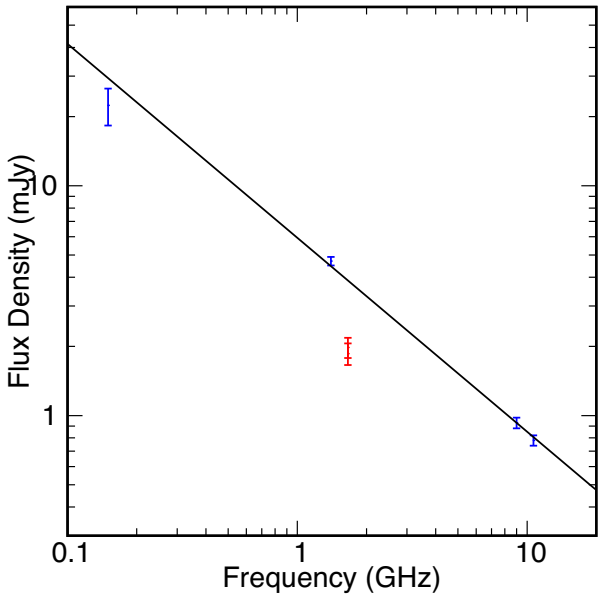

Figure 3. The broad-band radio spectrum of SDSS J090613.77+561015.2. The blue points are from the earlier total flux density observations by the VLA (Becker et al. 1995; Reines et al. 2020) and the GMRT (Intema et al. 2017). The two red points are from our high-resolution EVN observations. The black line shows the best-fitting power-law spectrum to the low-resolution total flux density measurements (blue points).

where $S_{\rm obs}$ is the observed total flux density in mJy, $\nu_{\rm obs}$ is the observing frequency in GHz, $\theta_{\rm size}$ is the full width at half-maximum (FWHM) of the circular Gaussian model in mas, and z is the redshift. The components N and S have average brightness temperatures of 1.2×10^8 and 7.1×10^6 K, respectively, at 1.66 GHz in the second-epoch 12-h full-EVN observations. Due to the very limited (u, v) coverage and the low image sensitivity, the component S has an underestimated $\theta_{\rm size}$ and thus an overestimated $T_{\rm b}$ in the first-epoch 2-h-long e-EVN observation.

4 DISCUSSION

4.1 The nature of the components N and S

The only plausible explanation of the radio structure in SDSS J090613.77+561015.2 appears to be an AGN manifestation. The optical spectroscopic observations of SDSS J090613.77+561015.2 show that there are no signatures for on-going star-forming activity in the BPT (Baldwin, Phillips & Terlevich 1981) diagrams formed with some emission-line ratios (Reines et al. 2020). The persistent broad Hα emission is consistent with an AGN origin (Baldassare et al. 2016). Therefore, we reject a possibility that the observed components represent a superposition of supernova remnants (SNRs) like in, e.g. Arp 220 (Varenius et al. 2019). Moreover, they cannot be explained as two young radio supernovae because of their radio structures resolved on the pc scales although their radio luminosities ($L_{\rm R} \sim 8 \times 10^{37}$ erg s^{-1}) are in the luminosity range of young radio supernovae (maximum: $L_{\rm R} \sim 5 \times 10^{38}$ erg s^{-1}, Weiler et al. 2002).

The component N is either the radio core, i.e. the jet base, or a newly emerging jet component. Its proximity (within the 1σ positional error) to the optical centroid of SDSS J090613.77+561015.2 is consistent with this hypothesis. There also exists a jet-like faint extension toward South in the component N when the image resolution in north–south is slightly improved to 4 mas. We can also fit the component N to two-point sources with flux densities 0.73 ± 0.02 and 0.19 ± 0.02 mJy and a separation of 3.9 ± 0.4 mas.

The component S is most likely an expanding ejecta. Because of its large distance (∼58.5 mas) to the *Gaia* centroid, it cannot be explained as the radio core. Compared to the component N, the component S has the more extended structure and the lower brightness temperature. Moreover, its position and elongation (position angle about 36°) are roughly aligned with the extension of the component N.

The *Gaia* positioning of the optical centroid close to the radio component N provides a strong indication on the nature of this component as the compact radio core. However, we cannot rule out that SDSS J090613.77+561015.2 is a young compact symmetric object (CSO, Wilkinson et al. 1994). In this scenario, the radio components N and S are a pair of moving-out radio ejectae (or mini-lobes) within its host galaxy, and the radio core is located somewhere in-between and undetected. The latter would be still consistent with the *Gaia* position within its 3σ error. Assuming a typical separation speed of $0.2c$ among CSOs (e.g. An et al. 2012), the pair of components would have a kinematic lifetime of $\sim 7.5 \times 10^2$ yr. This is a typical value in young extragalactic radio sources (e.g. An & Baan 2012). Steep spectra at $\gtrsim$1 GHz are not unknown among CSOs, e.g. J0132+5620 and J2203+1007 (An et al. 2012). Another example is the CSO PKS 1117+146, which has a spectral index of -0.7 (Torniainen et al. 2007) and a large angular separation between the opposite jet components, ∼70 mas (Bondi et al. 1998), and thus is similar to SDSS J090613.77+561015.2. A conclusive test on possible CSO identification of the source will be provided by its future multifrequency and multi-epoch VLBI studies.

4.2 Implications of the presence of a radio jet associated with the IMBH

If the component N is the stationary radio core associated with the IMBH, SDSS J090613.77+561015.2 will have a relatively high radio luminosity. The source has an X-ray luminosity of $L_{\rm X} = 4.5 \times 10^{40}$ erg s^{-1} in the 2–7 keV band (Baldassare et al.

2017). This leads to a ratio of $\frac{L_R}{L_X} = 1.8 \times 10^{-2}$, much higher than the typical value $\sim 10^{-5}$ in the radio-quiet Palomar–Green quasar sample (Laor & Behar 2008). Due to the high ratio, it is hard to explain them as wide-angle radio-emitting winds. At the low accretion rate state, there exists a correlation (e.g. Merloni, Heinz & Di Matteo 2003) between the radio core luminosity at 5 GHz, the X-ray luminosity (L_X) in the 2–10 keV band, and the BH mass (M_{bh}):

$$\log L_R = \left(0.60^{+0.11}_{-0.11}\right) \log L_X + \left(0.78^{+0.11}_{-0.09}\right) \log M_{bh} + 7.33^{+4.05}_{-4.07}. \quad (2)$$

According to equation (2), we would expect $L_R = 10^{36.1 \pm 0.9}$ erg s^{-1}. This estimate would be one order of magnitude lower while still in the acceptable range in view of the large scatter of the correlation.

The radio jet is rarely seen in dwarf galaxies. Compared to the first and only case, NGC 4395 (Wrobel & Ho 2006), SDSS J090613.77+561015.2 has a jet 160 times longer and 10^5 times more luminous. The finding of the large jet structure indicates that violent ejections might appear at the BH growth stage of $M_{bh} \sim 10^5$ M$_\odot$ in the early Universe. Most of these jets associated with low-mass BHs might be short-lived and sub-kpc objects because they have rather low radio luminosities ($L_R \leq 10^{41}$ erg s^{-1} at 1.4 GHz, Kunert-Bajraszewska et al. 2010; An & Baan 2012).

Manzano-King et al. (2019) report some AGN-driven outflows in dwarf galaxies, indicating significant AGNs impact on the large-scale kinematics and gas content. The kpc-scale high-velocity ionized gas outflows in SDSS J090613.77+561015.2 might be driven by the AGN jet activity, in particular the diffuse structure completely resolved out in our EVN image because of missing the shorter baselines. The unseen kpc-scale (relic) jet component has a flux density of 2.0 ± 0.2 mJy. According the scaling relation $P_{jet} = 5.8 \times 10^{43} (\frac{L_R}{10^{40}})^{0.70}$ erg s^{-1} between jet kinematic power and the radio luminosity derived by Cavagnolo et al. (2010) using *Chandra* X-ray and VLA radio data of radio galaxies, the unseen relic jet has a power of $P_{jet} = 10^{42.6 \pm 0.7}$ erg s^{-1}, reaching about 10 per cent of the Eddington luminosity $L_{Edd} = 10^{43.6 \pm 0.4}$ erg s^{-1} of the IMBH. Thus, the AGN jet activity might have significant impact on the host galaxy.

ACKNOWLEDGEMENTS

The European VLBI Network is a joint facility of independent European, African, Asian, and North American radio astronomy institutes. Scientific results from data presented in this publication are derived from the following EVN project codes: RSY05 and EY029. e-VLBI research infrastructure in Europe is supported by the European Union's Seventh Framework Programme (FP7/2007-2013) under grant agreement number RI-261525 NEXPReS. The research leading to these results has received funding from the European Commission Horizon 2020 Research and Innovation Programme under grant agreement No. 730562 (RadioNet). This work has made use of data from the European Space Agency (ESA) mission *Gaia* (https://www.cosmos.esa.int/gaia), processed by the *Gaia* Data Processing and Analysis Consortium (DPAC, https://www.cosmos.esa.int/web/gaia/dpac/consortium). Funding for the DPAC has been provided by national institutions, in particular the institutions participating in the *Gaia* Multilateral Agreement. LIG acknowledges support by the CSIRO Distinguished Visitor Programme. We thank the staff of the GMRT that made these observations possible. The GMRT is run by the National Centre for Radio Astrophysics of the Tata Institute of Fundamental Research. This research has made use of data from the OVRO 40-m monitoring programme (Richards et al. 2011) which is supported in part by NASA grants NNX08AW31G, NNX11A043G, and NNX14AQ89G and NSF grants AST-0808050 and AST-1109911.

REFERENCES

An T., Baan W. A., 2012, ApJ, 760, 77
An T. et al., 2012, ApJS, 198, 5
Baldassare V. F. et al., 2016, ApJ, 829, 57
Baldassare V. F., Reines A. E., Gallo E., Greene J. E., 2017, ApJ, 836, 20
Baldwin J. A., Phillips M. M., Terlevich R., 1981, PASP, 93, 5
Becker R. H., White R. L., Helfand D. J., 1995, ApJ, 450, 559
Bellovary J. M., Cleary C. E., Munshi F., Tremmel M., Christensen C. R., Brooks A., Quinn T. R., 2019, MNRAS, 482, 2913
Bondi M., Garrett M. A., Gurvits L. I., 1998, MNRAS, 297, 559
Cavagnolo K. W., McNamara B. R., Nulsen P. E. J., Carilli C. L., Jones C., Bîrzan L., 2010, ApJ, 720, 1066
Condon J. J., Condon M. A., Gisler G., Puschell J. J., 1982, ApJ, 252, 102
Gaia Collaboration, 2016, A&A, 595, A1
Gaia Collaboration, 2018, A&A, 616, A1
Greene J. E., Strader J., Ho L. C., 2020, ARA&A, preprint (arXiv:1911.09678)
Greisen E. W., 2003, in Heck A., ed., Astrophysics and Space Science Library, Vol. 285, Information Handling in Astronomy: Historical Vistas. Kluwer, Dordrecht, p. 109
Intema H. T., Jagannathan P., Mooley K. P., Frail D. A., 2017, A&A, 598, A78
Keimpema A. et al., 2015, Exp. Astron., 39, 259
Kormendy J., Ho L. C., 2013, ARA&A, 143, 511
Kunert-Bajraszewska M., Gawro'nski M. P., Labiano A., Siemiginowska A., 2010, MNRAS, 408, 2261
Laor A., Behar E., 2008, MNRAS, 390, 847
Ma C. et al., 1998, AJ, 116, 516
Manzano-King C., Canalizo G., Sales L. V., 2019, ApJ, 884, 54
Merloni A., Heinz S., Di Matteo T., 2003, MNRAS, 345, 1057
Paragi Z., Frey S., Kaaret P., Cseh D., Overzier R., Kharb P., 2014, ApJ, 791, 2
Pardo K. et al., 2016, ApJ, 831, 203
Reines A. E., Comastri A., 2016, PASA, 33, e054
Reines A. E., Deller A. T., 2012, ApJ, 750, L24
Reines A. E., Greene J. E., Geha M., 2013, ApJ, 775, 116
Reines A. E., Condon J. J., Darling J., Greene J. E., 2020, ApJ, 888, 36
Richards J. L. et al., 2011, ApJS, 194, 29
Schutte Z., Reines A. E., Greene J. E., 2019, ApJ, 887, 245
Shepherd M. C., Pearson T. J., Taylor G. B., 1994, BAAS, 26, 987
Thornton C. E., Barth A. J., Ho L. C., Rutledge R. E., Greene J. E., 2008, ApJ, 686, 892
Torniainen I., Tornikoski M., Lähteenmäki A., Aller M. F., Aller H. D., Mingaliev M. G., 2007, A&A, 469, 451
Varenius E. et al., 2019, A&A, 623, A173
Volonteri M., 2010, ARA&A, 18, 279
Weiler K. W., Panagia N., Montes M. J., Sramek R. A., 2002, ARA&A, 40, 387
Wilkinson P. N., Polatidis A. G., Readhead A. C. S., Xu W., Pearson T. J., 1994, MNRAS, 269, 67
Wrobel J. M., Ho L. C., 2006, ApJ, 646, L95
Yuan F., Narayan R., 2014, ARA&A, 52, 529

This paper has been typeset from a TEX/LATEX file prepared by the author.